AD-A136 134 DEVELOPMENT OF INNOVATIVE MILLIMETER-WAVE BROADBAND MIXERS(U) MICHIGAN UNIV ANN ARBOR ELECTRON PHYSICS LAB J CHEN ET AL. JAN 83 018223-F N00173-80-C-0118 1/1

UNCLASSIFIED F/G 9/5 NL

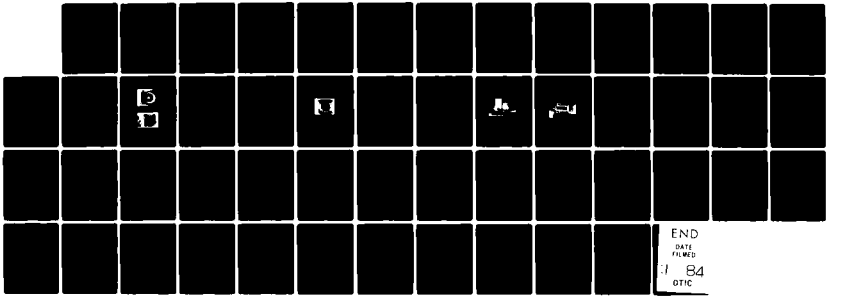

END
DATE FILMED
1 84
DTIC

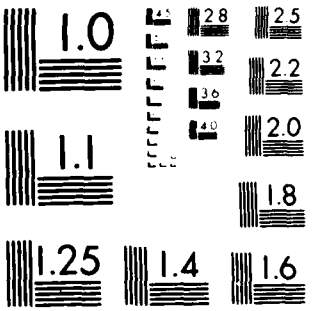

Report 018223-F

DEVELOPMENT OF INNOVATIVE MILLIMETER-WAVE BROADBAND MIXERS

J. Chen, J. R. East, and G. I. Haddad
Electron Physics Laboratory
Department of Electrical and Computer Engineering
The University of Michigan
Ann Arbor, MI 48109

and

Y. Anand, L. Mang, S. Ellis, and D. Densenouci
Microwave Associates, Inc.
60 South Avenue
Burlington, MA 01803

January 1983

Final Report for Period 24 March 1980 - 24 September 1982

Prepared for

NAVAL RESEARCH LABORATORY
Code 5251
Washington, DC 20376

UNCLASSIFIED

SECURITY CLASSIFICATION OF THIS PAGE (When Data Entered)

REPORT DOCUMENTATION PAGE		READ INSTRUCTIONS BEFORE COMPLETING FORM
1. REPORT NUMBER 018223-F	2. GOVT ACCESSION NO.	3. RECIPIENT'S CATALOG NUMBER
4. TITLE (and Subtitle) Development of Innovative Millimeter-Wave Broadband Mixers		5. TYPE OF REPORT & PERIOD COVERED Final Report 24 March 1980-24 Sept 1982 6. PERFORMING ORG. REPORT NUMBER
7. AUTHOR(s) J. Chen, J. R. East, G. I. Haddad, Y. Anand, L. Mang, S. Ellis, and D. Densenouci		8. CONTRACT OR GRANT NUMBER(s) N00173-80-C-0118
9. PERFORMING ORGANIZATION NAME AND ADDRESS Electron Physics Laboratory The University of Michigan Ann Arbor, MI 48109		10. PROGRAM ELEMENT, PROJECT, TASK AREA & WORK UNIT NUMBERS 62762N, F62581, 008
11. CONTROLLING OFFICE NAME AND ADDRESS Naval Research Laboratory Code 5251 Washington, DC 20376		12. REPORT DATE January 1983 13. NUMBER OF PAGES 45
14. MONITORING AGENCY NAME & ADDRESS(if different from Controlling Office)		15. SECURITY CLASS. (of this report) Unclassified 15a. DECLASSIFICATION/DOWNGRADING SCHEDULE N/A

16. DISTRIBUTION STATEMENT (of this Report)

Approved for public release; distribution unlimited.

17. DISTRIBUTION STATEMENT (of the abstract entered in Block 20, if different from Report)

18. SUPPLEMENTARY NOTES

19. KEY WORDS (Continue on reverse side if necessary and identify by block number)

Millimeter-wave mixers and detectors
BARITT devices
TUNNETT devices
Burnout
Schottky-barrier mixers
Conversion loss

20. ABSTRACT (Continue on reverse side if necessary and identify by block number)

The theoretical and experimental characteristics of BARITT and TUNNETT devices for use as millimeter-wave mixers and detectors were investigated. Theoretical calculations of BARITT conversion loss, noise figure, and RF and IF impedance levels were carried out. BARITT device fabrication was studied. Three BARITT structures, useful for frequencies between 35 and 95 GHz were fabricated and tested. BARITT devices were tested as mixers and detectors at 35 and 95 GHz. BARITTs were found to be useful millimeter-wave mixers or detectors. BARITT detector performance is comparable to more conventional

DD FORM 1 JAN 73 1473

UNCLASSIFIED

SECURITY CLASSIFICATION OF THIS PAGE (When Data Entered)

20. (Cont.)

detectors with TSS levels of - 48 dB per 1 MHz bandwidth and a dynamic range to 1-dB compression of 40 dB. The BARITT pulse burnout performance is superior to any conventional detector with a pulsed burnout level greater than 45 W.

BARITT mixer performance is also comparable to Schottky-barrier mixers with conversion losses of 5 dB and 30 MHz noise figures of 6.8 dB. This performance, coupled with the high burnout level and ease of fabrication, makes the BARITT a useful millimeter-wave device.

TABLE OF CONTENTS

LIST OF ILLUSTRATIONS

1. INTRODUCTION

The purpose of this program was to evaluate BARITT and TUNNETT devices for use as mixers and detectors in the 30- to 110-GHz frequency range. Both theoretical and experimental investigations were carried out and the results are described here. The theoretical considerations are given in Section 2 and the fabrication of BARITT devices is covered in Section 3 of this report. The cavities and circuits used to evaluate the BARITTs are discussed in Section 4. Experimental mixer and detector results are given in Section 5. Fabrication processes and experimental results for GaAs TUNNETT devices are given in Section 6 and an overall summary of the project is given in Section 7.

2. THEORETICAL CONSIDERATIONS

The theoretical results were presented in detail in a separate technical report.[1] This report was submitted to the project monitor. A theoretical study of frequency conversion and noise in millimeter-wave transit-time devices was carried out and the results were presented in this report. In particular the performance of BARITT devices as mixers and detectors in the 30- to 110-GHz range was studied. The RF and IF impedances of a wide range of BARITT structures were calculated. The excess RF voltage required for

---

1. Grondin, R. O., "Frequency Conversion and Noise in Millimeter-Wave Transit-Time Devices," Ph.D. Dissertation, The University of Michigan, 1982.

avalanche breakdown was also calculated. This information was used to choose device parameters for mixers and detectors.

The performance of BARITT mixers was based on a matrix formulation of frequency conversion and noise in transit-time devices. This matrix formulation was developed by extending conventional Schottky-barrier mixer models. Various burnout mechanisms and video detection were also considered. The results indicated that the BARITT will be competitive with Schottky-barrier diodes in low-noise video detection and mixer applications where high burnout capability and reasonable sensitivity are needed.

3. BARITT DEVICE FABRICATION

The wafer preparation and the fabrication steps developed to produce BARITT devices are described in this section. Three types of BARITT structures were designed and fabricated: the self-aligned structure, the polyamide structure and the multijunction structure. The initial fabrication steps for the first two structures are the same. The fabrication process starts with the formation of a junction in n-p^+ epitaxial Si wafers. The doping and epitaxial layer thickness are chosen based on the theoretical results of the computer models. Junctions can be formed either by diffusion to form a second p^+-n junction or by Schottky-barrier fabrication. Boron was used to form p^+ layers and platinum was used to form Schottky contacts. The p^+-n junctions always produced better mixer and detector performance than the Schottky contacts.

The second step in the process is wafer thinning. There are two reasons for wafer thinning. First, the excess substrate

material, if not removed, would contribute a lossy series resistance which would degrade the device performance. Second, the thinned wafer can be formed easily into individual diodes without scribing. Isotropic acid chemical etching is used to thin the wafer. A solution of HF, NHO_3 and CH_3COOH is used. The wafer is waxed onto a Teflon float with a quartz window on the bottom. CO_2 gas is bubbled into the etching solution from below. The bubbles agitate the solution, preventing large reaction bubbles from forming and leading to a more uniform etching process. The bubble etcher is shown in Figure 1. When the wafer becomes thinner than 20 μm its thickness can be judged by the color of light transmitted through it. The transmitted light is observed through the transparent quartz window in the float. The final wafer thickness is between 5 and 20 μm, depending on the remaining process steps being used. After etching, the wafer is removed from the float by heating to melt the wax. The wafer is then carefully cleaned and is ready for further processing.

3.1 Self-Aligned Structure.

The processing steps for the self-aligned structures are shown in Figure 2. Chrome and gold contact metals are deposited onto the thinned Si wafer, shown in Figure 2a. The wafer is then waxed onto a glass slide, with the substrate side exposed. Chrome and gold are deposited and a photoresist pattern of holes is exposed and developed onto the exposed wafer. The diameter of the photoresist holes is slightly larger than the final diameter of the diode mesa. A 5-μm thick layer of gold is electroplated through the holes. The gold on the wafer under the photoresist gives a current path for the plating. This structure is shown in Figure 2b. The wafer is then removed

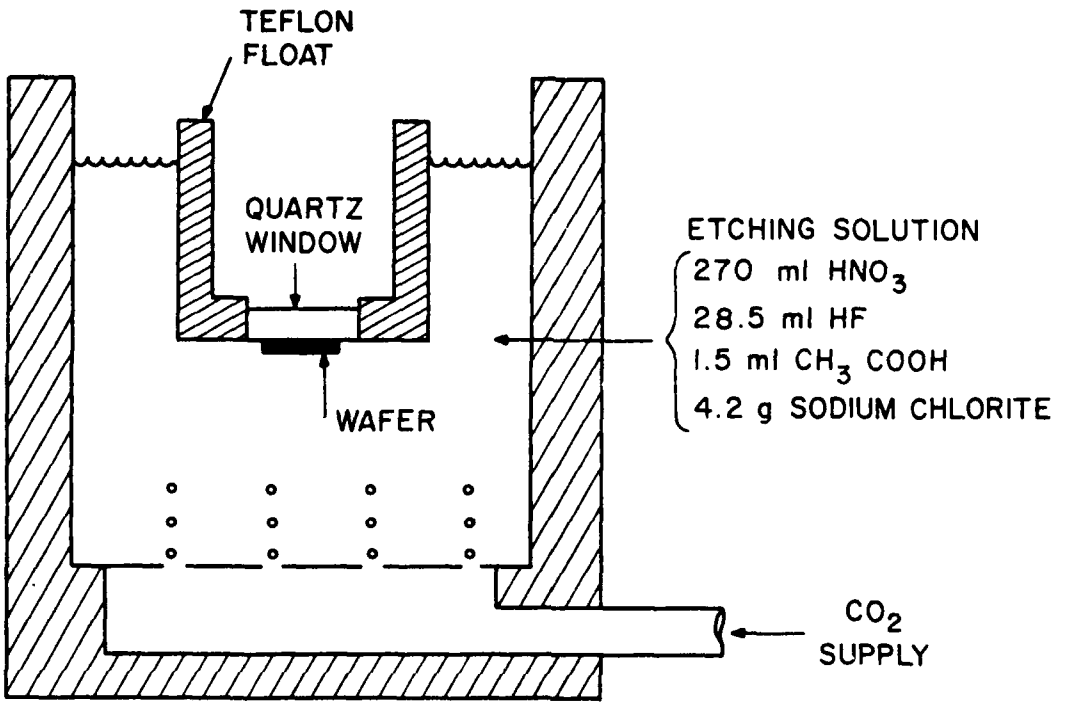

Figure 1. Bubble etcher geometry.

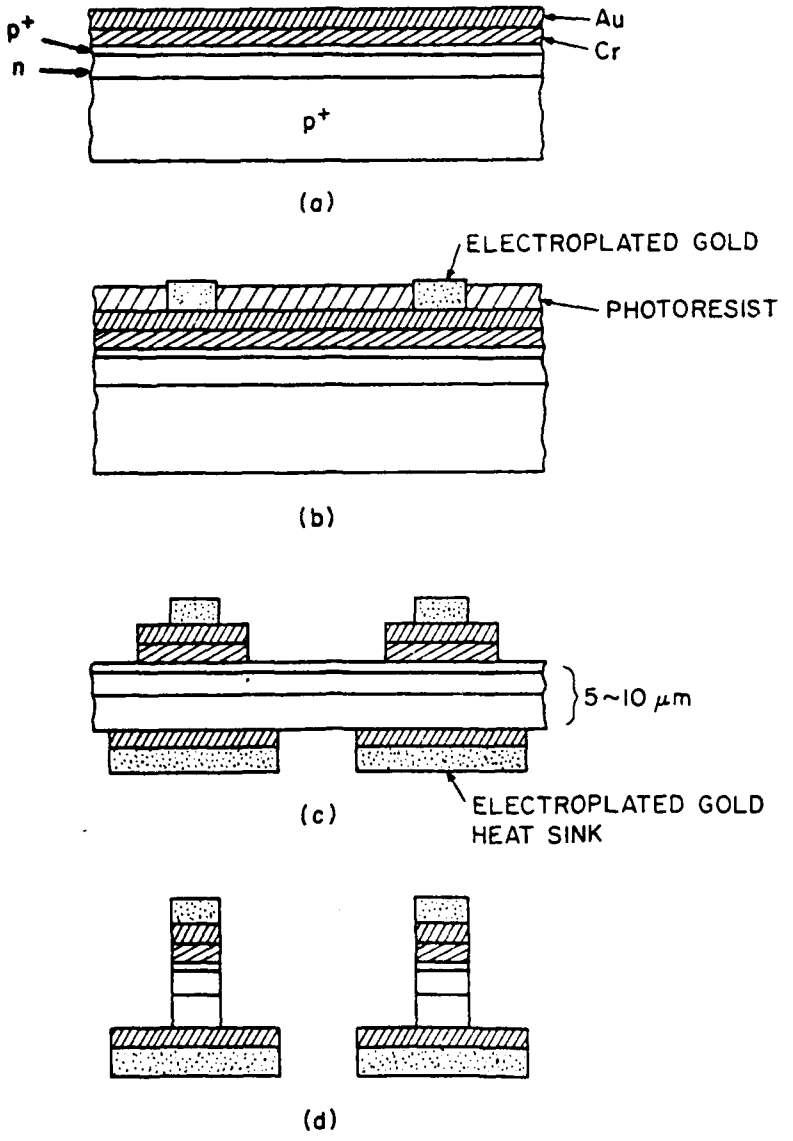

Figure 2. Self-aligned structure process.

from the glass slide, cleaned, turned over, and remounted onto the slide. The same plating process can be used to plate the heat sink pads. However, the heat sink pads must align with the mesa pads on the opposite side. Opposite corners of the wafer are immersed into gold, chrome, and Si etch to expose some of the plated pads. The exposed portions of the device pattern can be used to align the mask for the electroplated gold heat sinks. The pattern is illustrated in Figure 3. The structure after heat sink plating is shown in Figure 2c. The wafer is removed from the slide, cleaned, and rewaxed to another slide. The gold, chrome, and Si are then etched from between the plated mesa dots. The plated gold protects the area of the mesa. The final structure is shown in Figure 2d. The individual diodes are removed from the glass slide by placing the slide into a small basket and immersing it in trichloroethylene. This dissolves the wax and allows the diodes to drop to the bottom of the basket. After further cleaning and drying the diodes are ready to be bonded into packages for microwave testing. The gold heat sink pad is thermocompression bonded onto the heat sink mount of a minipill package. A 0.0007-inch diameter gold wire is bonded to the top contact.

3.2 Polyamide Structure

The self-aligned structure discussed in Section 3.1 requires a package for use in a test circuit. This presents a major problem at higher frequencies. The minipill package used for the self-aligned structure is approximately the same size as the V-band waveguide. This problem can be alleviated by using the bias post of the waveguide circuit to directly contact the diode chip.

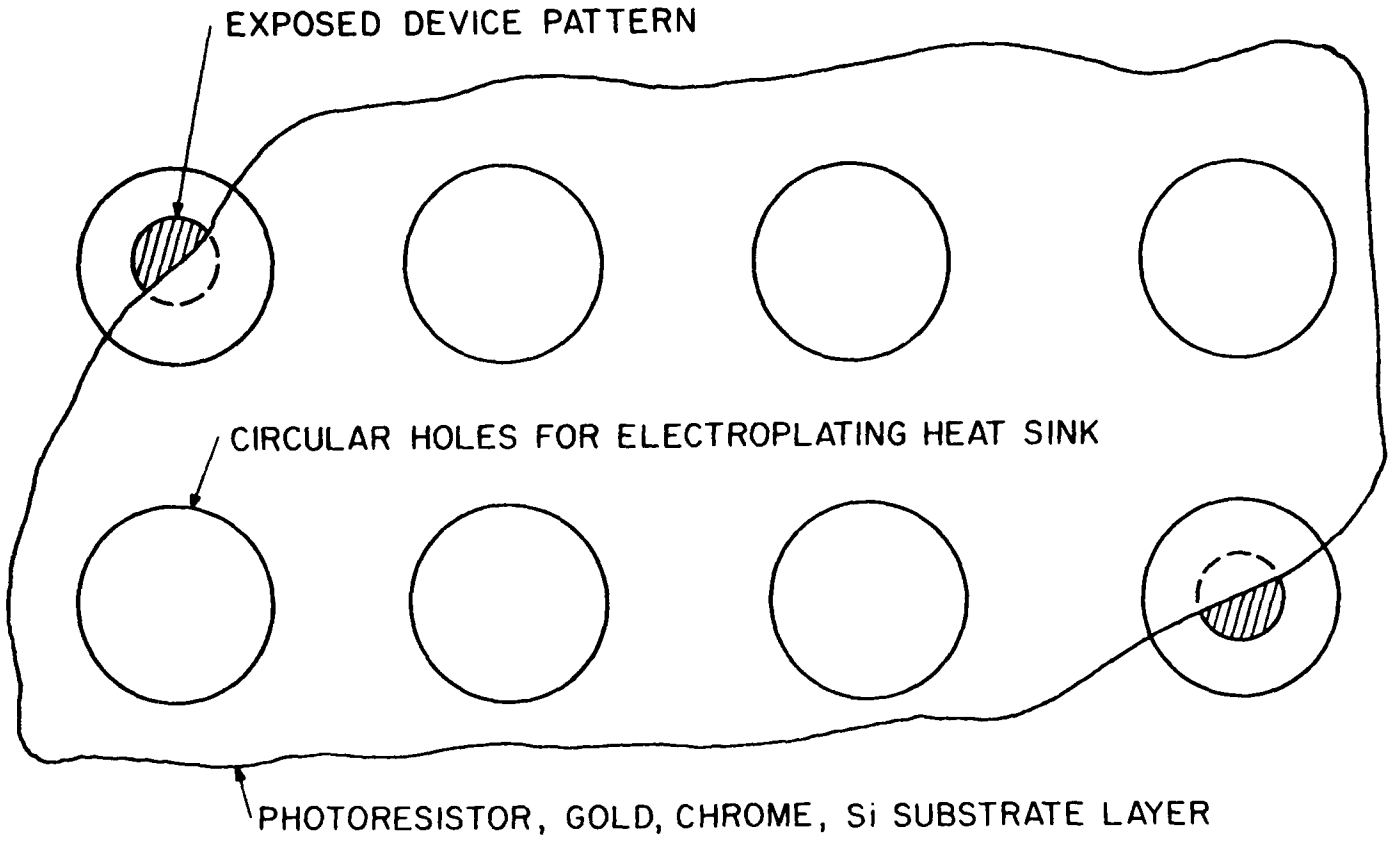

Figure 3. Heat sink etch geometry.

A polyamide standoff structure is used around the diode. The standoff prevents the post from crushing the diode upon contact. A photograph of the polyamide device is shown in Figure 4. The polyamide fabrication process is shown in Figure 5. The starting p^+-n wafer is cleaned and a thin thermal oxide is grown. A photoresist pattern of 0.002-inch diameter contact holes is exposed and developed onto the surface. This pattern is used to etch contact holes in the oxide. After etching the contact holes a thin layer of Pt is sputtered onto the surface and photoresist. The photoresist layer is then used to lift off the Pt except in the contact holes. The Pt is annealed in a forming gas atmosphere at 450°C for 10 minutes to form a Schottky barrier. The structure at this point is shown in Figure 5a. The next step is to define the polyamide structure on the top of the device. A ring-shaped pattern with an inner diameter of 0.002 inch and an outer diameter of 0.010 inch is used. The polyamide is spun onto the wafer, defined using a photoresist pattern, and etched using AZ photoresist developer. The resulting pattern is shown in Figure 5c. After a chrome-gold metallization, a photoresist layer is used to define a plating pattern for contact pads on the top of the diode. After a top contact plating, the structure is as shown in Figure 5d. After the remaining chrome and gold has been removed from the top side, the wafer is turned over, thinned, cleaned, and evaporated with chrome and gold on the backside. The corners are then etched, a plating photomask is defined, and the heat sink pads are plated. The structure at this point is shown in Figure 5e. The final mesa structure is formed by etching through the Si from the heat sink side, undercutting the heat sink slightly.

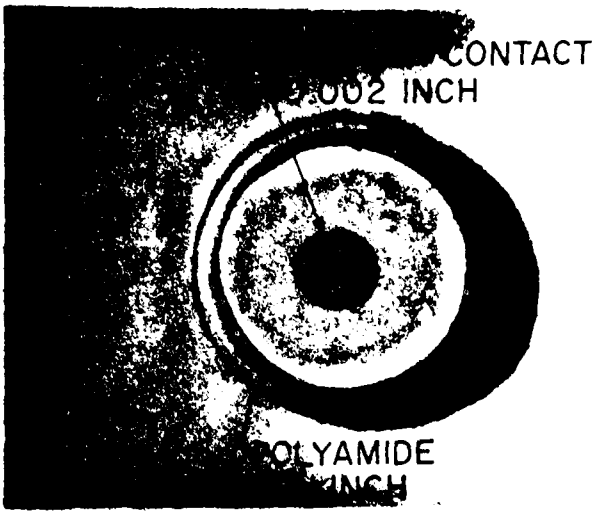

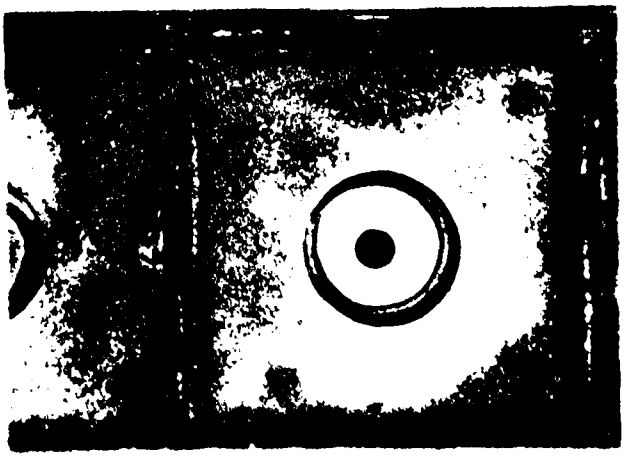

Figure 4. Polyamide device.

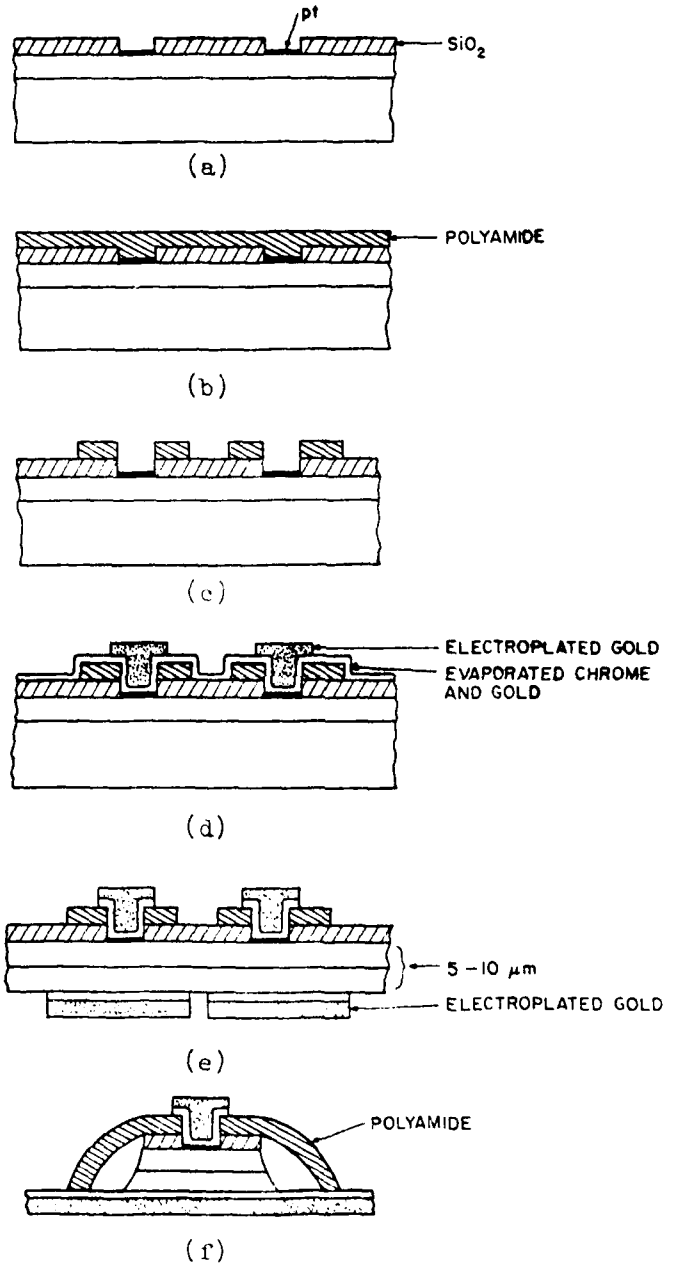

Figure 5. Polyamide device process.

The devices are removed from the slide and cleaned. They are then ready for RF testing.

3.3 Multijunction Structure

The multijunction structure is shown in a photograph in Figure 6. Instead of having one diode per chip, the contacts of this diode are in a honeycomb array with either 24 or 36 contacts per mesa. A pointed whisker is used as a contact. The process steps used to fabricate multijunction devices are shown in Figure 7. Chemical vapor deposition (CVD) is used to deposit a layer of SiO_2 on the surface of the starting n-p^+ epitaxial material. Initial attempts at multijunction fabrication used a thermal oxide. However, the oxidation process caused the p^+ substrate to outdiffuse into the n-layer, lowering the n-layer concentration and producing devices with high resistance. After the CVD step, a photolithography step is used to etch contact holes in the oxide. A short boron diffusion is used to form a p^+ contact on the surface. Chrome-gold contacts are then deposited into the contact holes. The oxide etch mask can also be used as a lift-off pattern for the contact metal pattern. The structure at this point in the process is shown in Figure 7c. The wafer is next thinned, metallized, and gold plated using the backside process discussed in Section 3.1. This structure is shown in Figure 7d. The individual diodes are formed by etching from the heat sink side. The mesa structure is overetched, allowing undercutting of the gold heat sink. The individual diodes are removed from the glass etching slide and cleaned. They are then ready to be thermocompression bonded onto a stud for RF testing. The heat sink undercutting at the mesa etch step leaves a thin

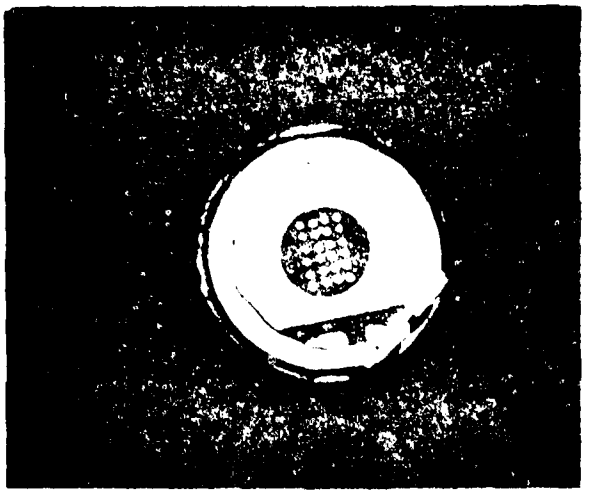

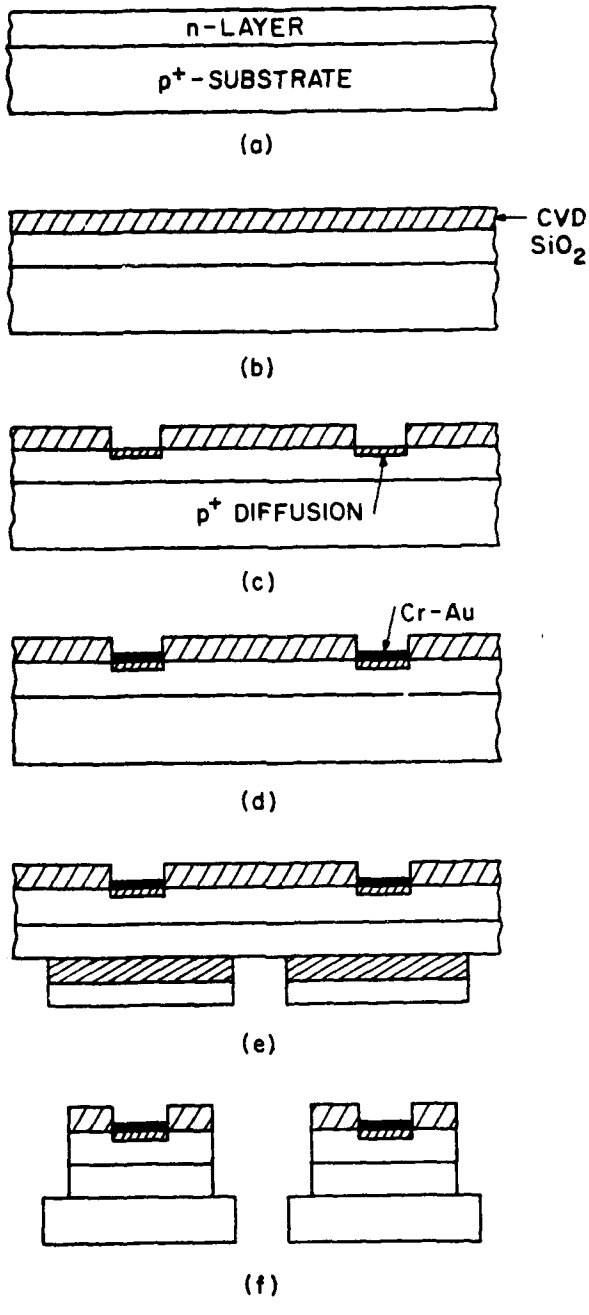

Figure 7. Multijunction device process.

rim of exposed heat sink on the chip, allowing space for the thermocompression bonding.

4. MIXER AND DETECTOR EXPERIMENTAL CIRCUITS

Several mixer and detector circuits were fabricated to test the BARITT devices. However, the best results were obtained in two circuits, one in the 26- to 40-GHz frequency range and one at 95 GHz.

The 35-GHz measurements were made in a ridged waveguide circuit. The circuit was designed to use BARITT devices packaged in minipill packages. The gap between the top of the waveguide ridge and the top of the waveguide is equal to the package height. A back short with a ridge cutout is used to tune the diode. The waveguide mixer circuit is connected to the rest of the waveguide circuit with a taper section. A bias post is used to bias the diode. The IF port, built as part of the bias post, is a five-section TEM coaxial waveguide trap. The wavetrap-bias post fits through a hole in the top of the cavity. The post is insulated from the cavity body by a thin dielectric sleeve. The cavity and IF choke assembly are shown in Figure 8.

The 95-GHz cavity is shown in Figure 9. This cavity is a full-height waveguide cavity designed for use with the multijunction honeycomb structure. The dimensions of this cavity are too small for a coaxial TEM IF choke. The cavity has a 0.010-inch diameter tungsten bias post with a 10-μm diameter point on the diode end. The bias post passes through a 30-Ω section one quarter wavelength long on the top of the waveguide. Above the quarter-wave section

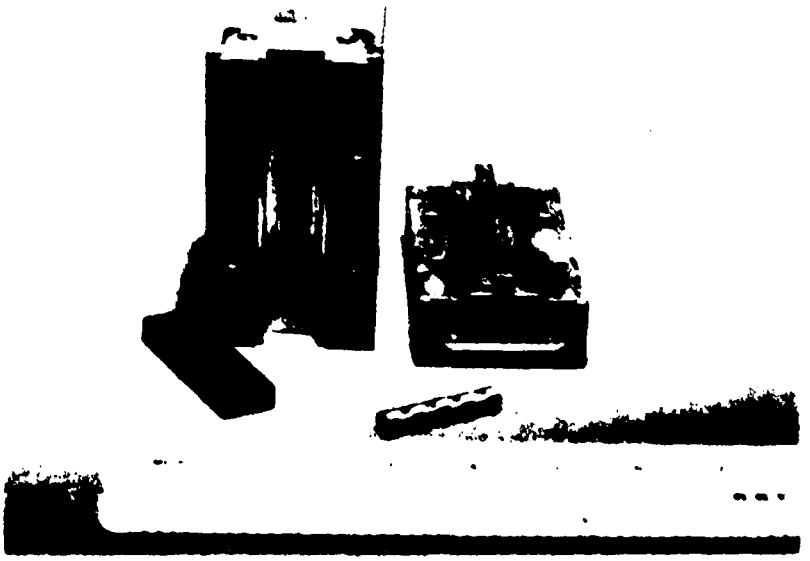

Figure 8. 35-GHz waveguide cavity.

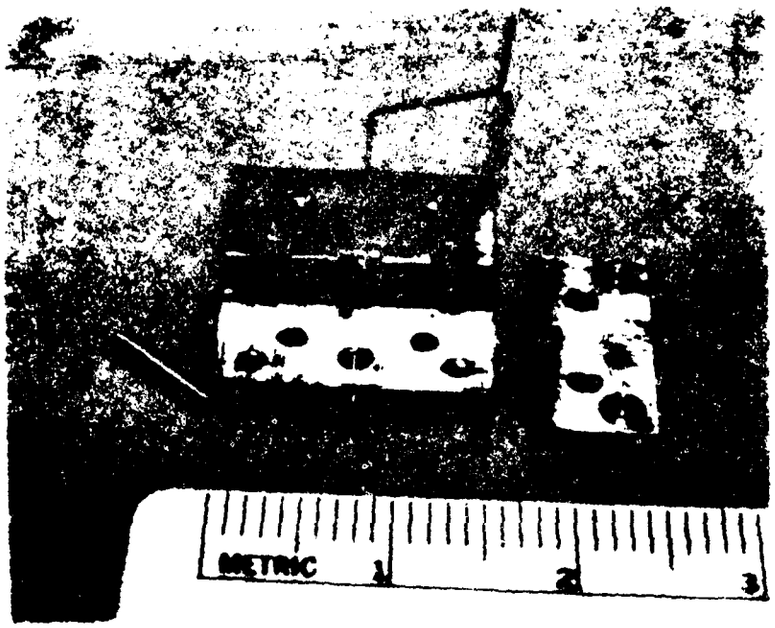
METRIC
1
2
3

is a radial choke centered at 95 GHz. The radial choke quarter-wave transformer combination provides a short circuit at the top of the waveguide at 95 GHz. The diode chip is silver epoxied to a pin which fits into the bottom of the cavity. The cavity is built as a split block structure. When the front of the block is removed, a small mirror can be placed into the bottom of the waveguide slot. When the bias pin is pushed into contact with the diode chip, the mirror can be used to place the diode in the best position.

Standard test circuits were used to measure BARITT mixer and detector performance. The TSS of the detectors and the conversion loss and noise figure of the mixers were measured. The pulsed RF burnout level was also measured. The detector test circuit is shown in Figure 10. A 1-kHz square-wave modulated test signal is applied to the detector through a variable attenuator. The portion of the test signal is sampled with the directional coupler and measured with the power meter. The detected 1-kHz signal is amplified with a low-noise amplifier and displayed on an oscilloscope. The test channel attenuation is adjusted until the TSS point is obtained. There were problems with this measurement circuit because of the high video impedance of the BARITT diode. The BARITT diode has a video impedance of approximately 1000 Ω for the bias current levels being used. A typical Schottky-barrier detector video impedance is much lower. Several low-noise amplifiers with different input impedance levels were tested in the detector circuit. The best results were obtained with a high input impedance amplifier. The bandwidth was 1 MHz.

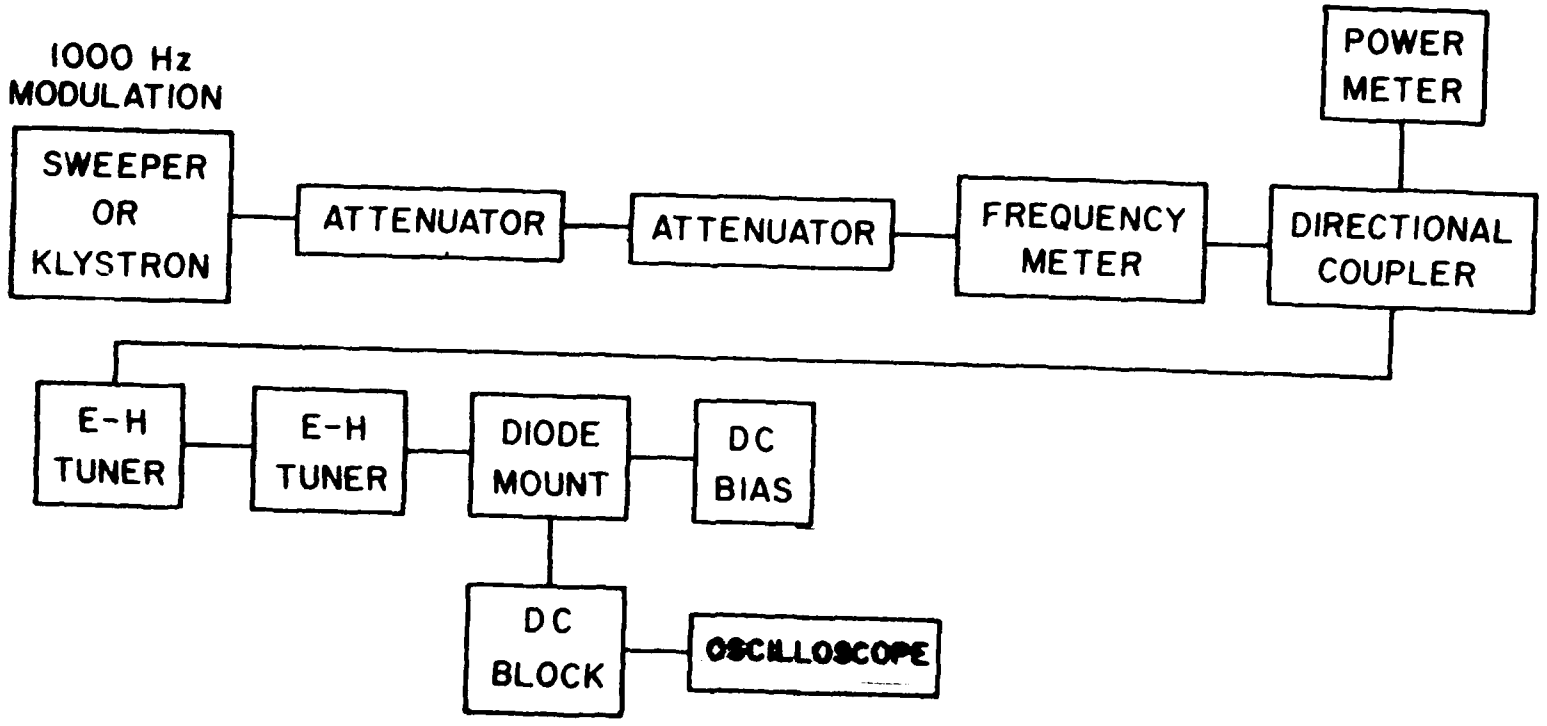

Figure 10. Detector test circuit.

The mixer test circuit is shown in Figure 11. A Gunn diode oscillator is used to pump the mixer. The pump signal is applied to the mixer through a directional coupler to provide isolation. Either a second signal source or a noise source is connected to the main line of the test circuit. For conversion loss measurements a signal frequency chosen to give the desired IF was applied. The power level of either the signal or the pump frequency could be measured using the power meter by increasing the attenuation of the other signal. The IF output level was measured using a spectrum analyzer as a calibrated receiver. The IF circuit was a 50-Ω system. Since video impedance problems were found in the detector measurements, similar problems were expected in the mixer measurements. A variety of tuning and matching circuits were tried between the mixer and the spectrum analyzer. However, this tuning did not improve the performance. In the noise figure measurement setup the signal source is replaced by a square-wave modulated excess noise source. The calibrated excess noise of the noise source, reduced by the loss into the load of the directional coupler, is applied to the mixer. The IF portion of the circuit uses a Y-factor measurement to find the mixer noise figure. The IF output signal of the mixer is amplified using a 30-MHz narrow-band amplifer. The signal is detected and displayed on an oscilloscope. Because of the dc block in the bias circuit the detected output is not a square wave. The signal is a decaying exponential with the time constant depending on the capacitance of the dc blocking capacitor. The Y-factor can be read off the oscilloscope from the leading edge of the pulse.

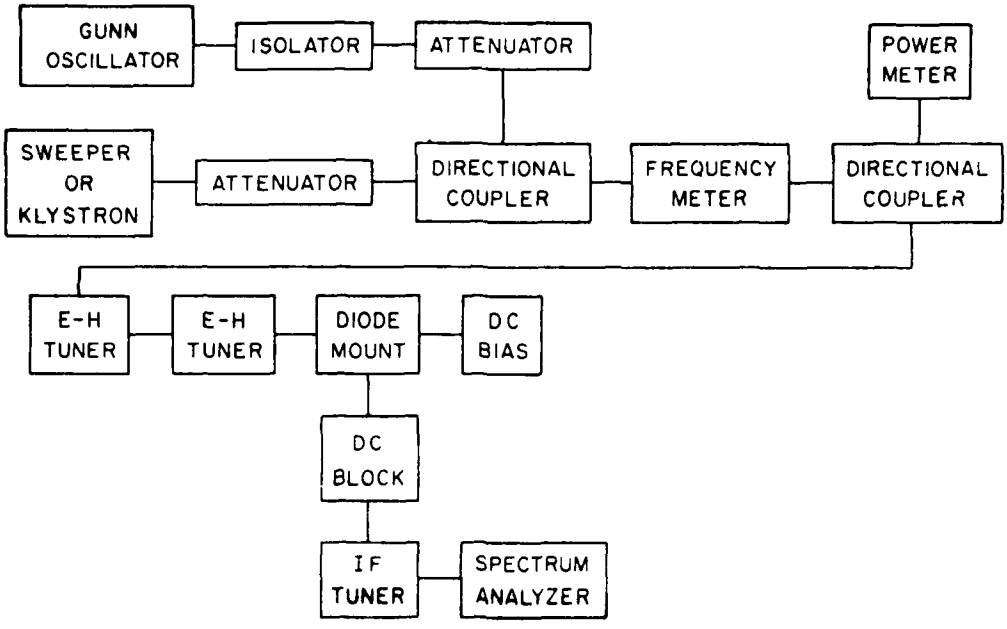

(a)

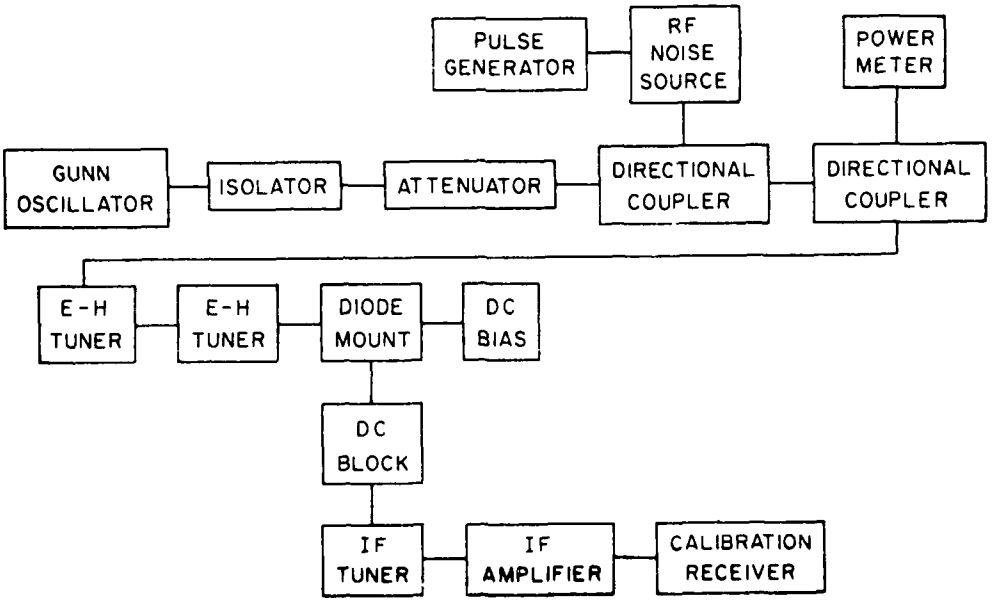

(b)

Figure 11. Mixer test circuit. (a) Conversion loss and (b) noise figure.

Since the pulse shape is not a square wave a noise figure meter cannot be used for the measurement.

The RF pulse burnout measurement setup is shown in Figure 12. The pulsed high-power output from the magnetron was attenuated and applied to the diode. The diode was tuned to the best small-signal detection point at the start of the test. The test power level was increased until the diode was damaged. After each series of power levels the power was lowered and the TSS was remeasured as a damage check.

The diodes fabricated using the techniques discussed in the previous section were tested to determine BARITT mixer and detector performance. These results are given in the next section.

5. MIXER AND DETECTOR EXPERIMENTAL RESULTS

A wide variety of BARITT devices has been fabricated and tested. The early structures used a long drift region and low doping. The performance was improved by making shorter more heavily doped devices. A short summary of the overall results is given. After the summary a more detailed description of the best devices is given.

The first diodes fabricated were used to study the effect of epitaxial layer thickness and device size on detector performance. The epitaxial layer resistivity was 2 Ω-cm. The detector characteristics for these devices are shown in Table 1. For this group of diodes the 2-μm devices were 10 dB better than the 4-μm devices. Except for the 4-μm group the larger diodes have better performance than the smaller ones. These devices were tested using bonded diodes in minipill packages. A modified coaxial package and a multijunction

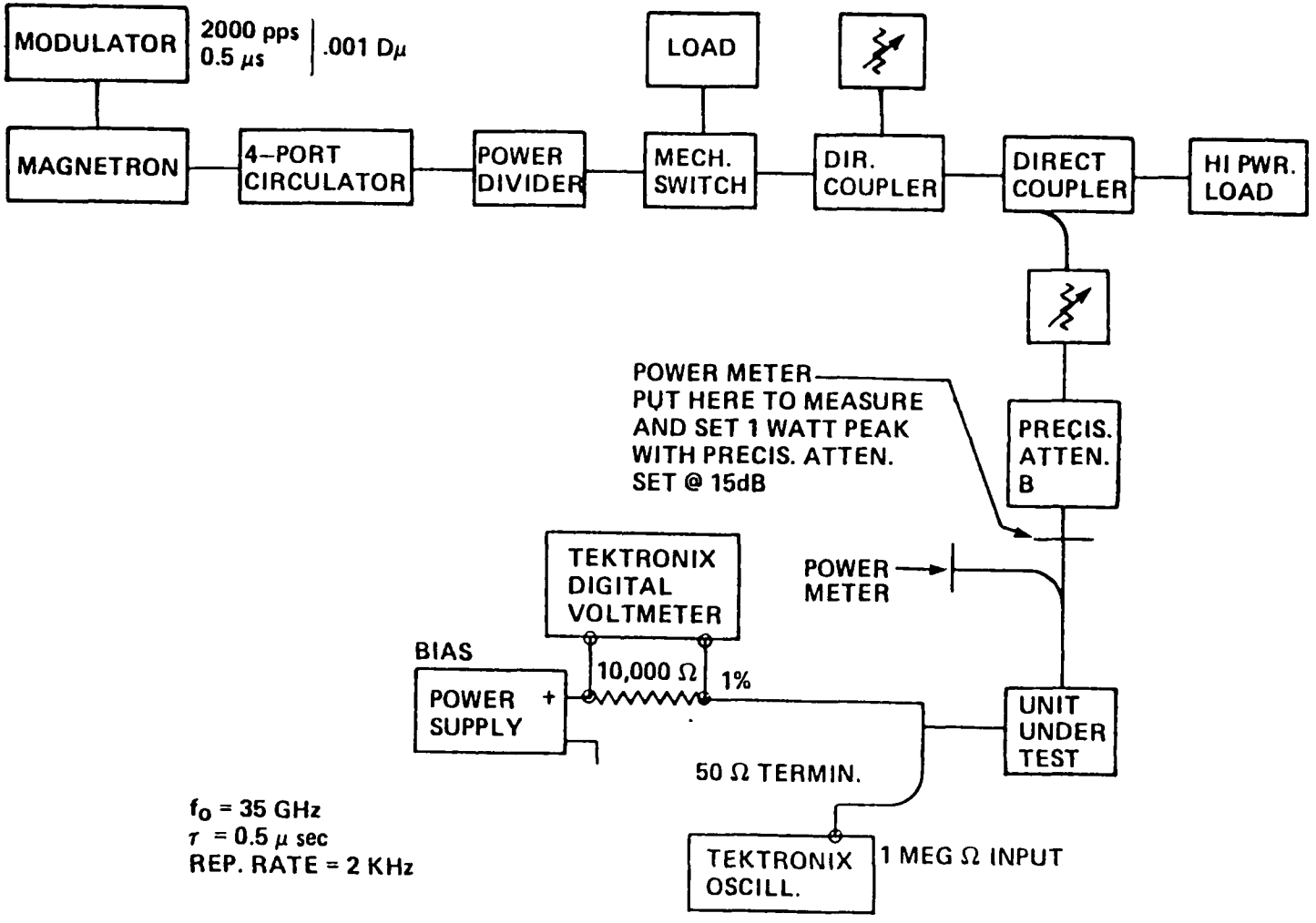

Figure 12. Pulse burnout measurement circuit.

TABLE 1. BARITT DETECTOR PERFORMANCE

Epitaxial Thickness (μm)	Window Size (μm)	TSS (35 GHz, 10 μA, Bw = 2 MHz) (dBm)
2	10	- 38
2	5	- 33
3	10	- 35
3	5	- 31
4	10	- 27
4	5	- 29

structure were also tested. However, the results were similar to the minipill package results. The devices were also tested over a range of bias currents. Results were always best for bias currents between 10 and 20 μA. The TSS is approximately 10 dB worse at 500 μA. This set of results shows a problem with BARITT devices. The video impedance level of a Schottky-barrier diode can be matched to the IF circuit by changing the bias current level. The video impedance of a BARITT is higher than a Schottky diode and less sensitive to bias current. The video impedance of a 3-μm BARITT structure is shown in Table 2. Increasing the bias current beyond 200 μA does not further decrease the video impedance. Video impedances this high make IF signal processing difficult.

The major reason for high video impedances is space-charge resistance in the reverse-bias portion of the diode. The low field region of the device must have a relatively high carrier concentration to support the current flow. When the hole concentration becomes comparable to the background doping the field and applied voltage must rise and the space-charge resistance increases. With this explanation for the early results more devices were fabricated with thinner and more heavily doped epitaxial layers.

The best mixer and detector results were obtained with thin heavily doped epitaxial layers. The last group of devices tested had an epitaxial layer thickness of 1 μm and a doping of 10^{16} cm^{-3}. The 33-GHz detector and mixer devices were self-aligned structures mounted in minipill packages. The best results were obtained with devices approximately 25 μm in diameter. The self-aligned structure is fabricated with a diameter of approximately 50 μm. The devices

TABLE 2. BARITT VIDEO IMPEDANCE

Bias Current (μA)	Video Impedance (Ω)
20	4400
50	4300
100	3500
200	2800

were tested with this diameter and then etched to a smaller diameter in small steps. There was a continuous improvement as the diameter was reduced. However 25-μm diameter structures are the smallest structures that could be fabricated. The optimal diameter appears to be smaller than 25 μm and larger than the 10-μm structures discussed earlier. It was hoped that even thinner more heavily doped structures could be tested. However, this combination of doping and thickness on a p^+ substrate poses problems in epitaxial growth. During the epitaxial growth a change from heavily doped p material to heavily doped n material is occurring. For thinner heavily doped structures the transition region requirements are tighter. The present growth system has a transition region approximately 1 μm thick. The 10^{16} cm^{-3} doping level is a nominal value, with a graded lower doped region at the epitaxial layer-substrate interface. Additional work is necessary to solve this problem.

BARITT diode detector performance is shown in Figures 13 through 16. Figure 13 shows the TSS performance of a 25-μm diameter device operating at 32 GHz. The TSS performance of the same device operating between 26 and 40 GHz is shown in Figure 14. The center frequency of the device depends on the IF wave trap being used. The output voltage vs. input power level is shown in Figure 15. BARITT detector performance is comparable to Schottky-diode detectors. Commerical 35-GHz Schottky detectors have TSS values between - 45 and - 50 dBm, as compared with - 48 dBm shown in Figures 13 and 14. Commercial Schottky detectors have a square-law dynamic range of approximately 30 dB. The dynamic range shown in Figure 15 is 40 dB. BARITT operation under large pulsed power conditions is

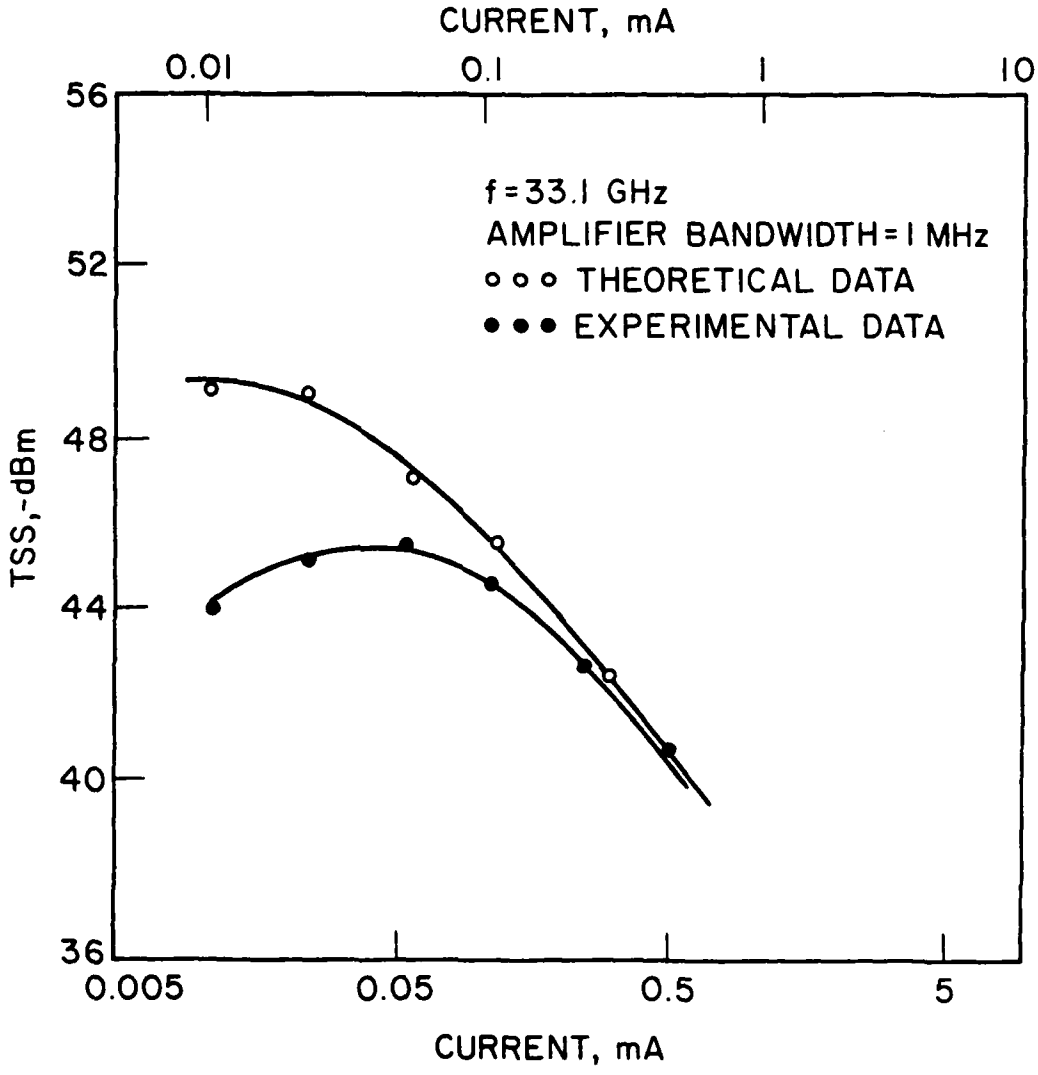

Figure 13. BARITT diode TSS performance.

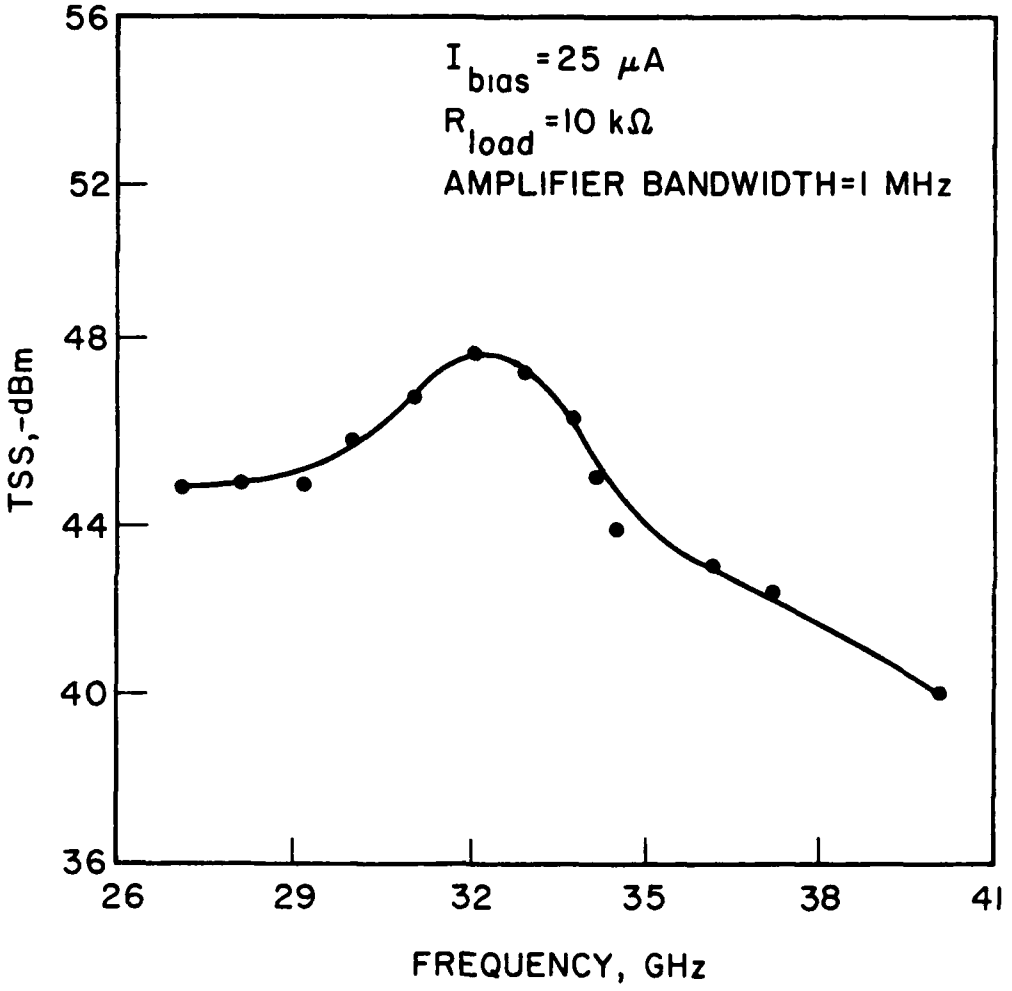

Figure 14. BARITT detector performance vs. frequency.

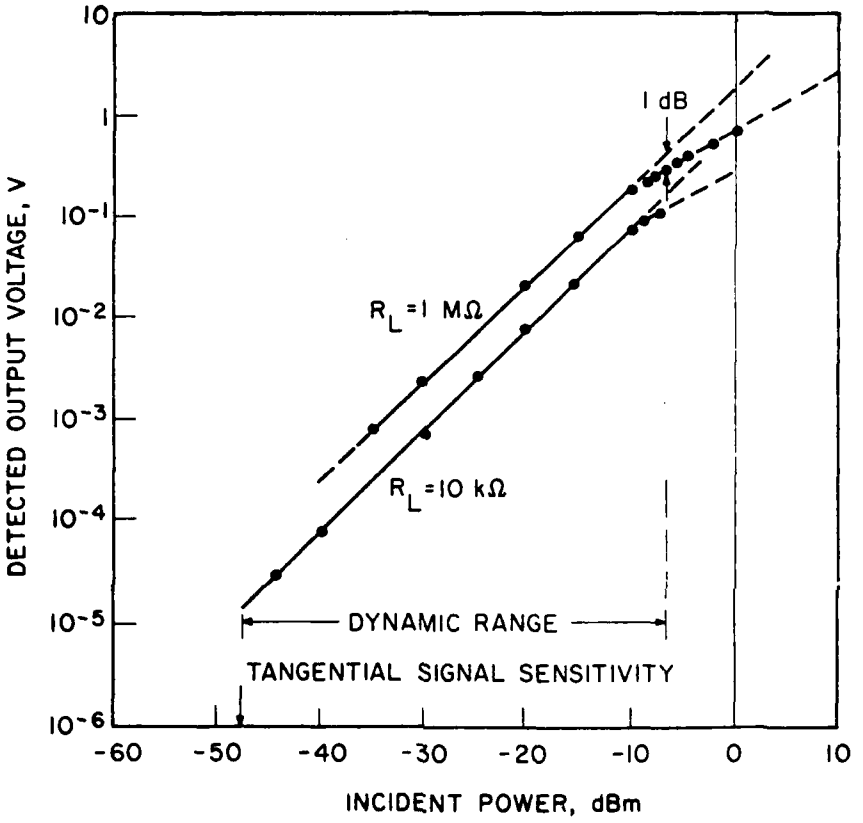

Figure 15. BARITT detector dynamic range measurement.

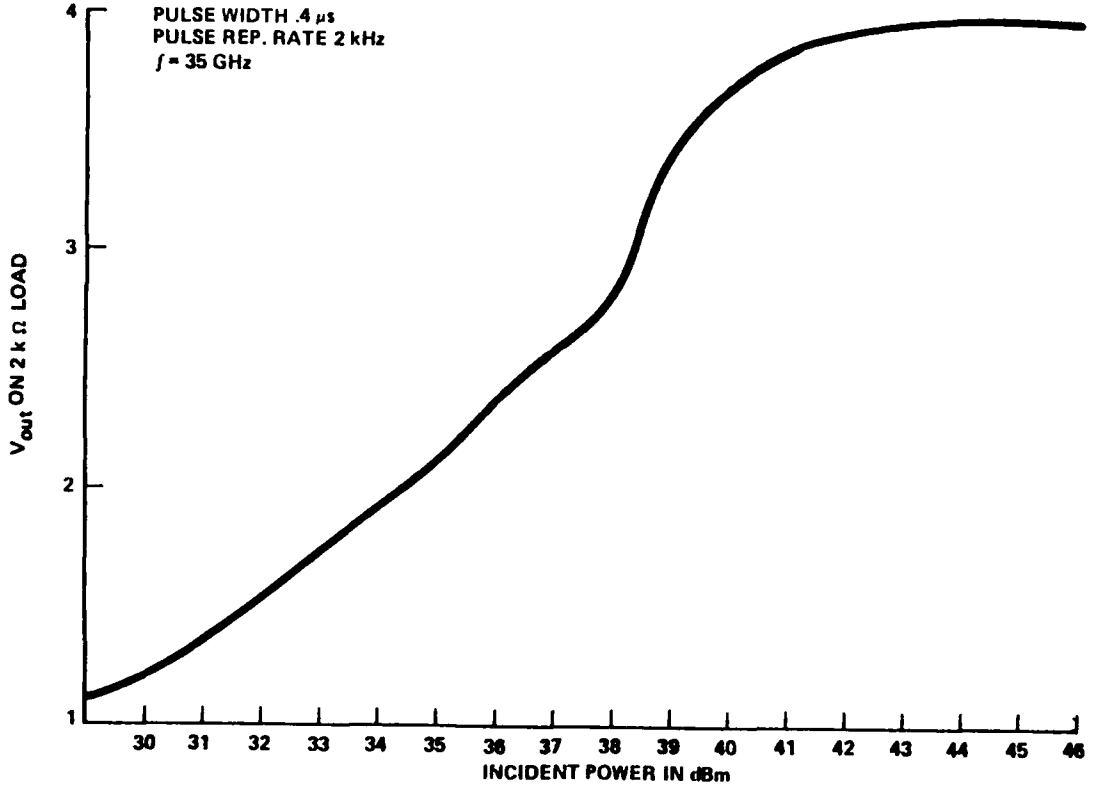

Figure 16. BARITT detector burnout measurement.

shown in Figure 16. The diode shown in Figure 16 withstood pulsed power levels greater than 45 W, the power limit of the measurement system. This power level is much higher than the power limits of Schottky-barrier devices.

The information in Figures 13 through 16 shows that Si BARITT diodes have great potential as millimeter-wave detectors. They have good TSS performance and have burnout characteristics and square-law dynamic range superior to Schottky detectors. The devices are larger and are easier to fabricate and bond. Further work is needed on the Si epitaxial material to increase the epitaxial layer doping and to improve the transition between the substrate and the epitaxial layer. Another approach to improve the substrate epitaxial layer interface would be to switch from Si to GaAs. GaAs can be grown with a variety of low-temperature processes and has much better doping control than Si. Additional work would be necessary to find the performance limits of GaAs BARITTs.

The best mixer results were obtained with the 1-μm and 10^{16} cm^{-3} doping devices. The same devices gave good mixer and detector results. BARITT mixer performance is shown in Figures 17 through 21. Figure 17 shows the conversion loss of a 32.3-GHz BARITT mixer operating with a 30-MHz IF. Figure 18 shows the conversion loss with a 150-MHz IF. For these measurement conditions the conversion loss was the same with the signal frequency above or below the pump frequency. Over a 2- to 6-mA bias current range the conversion loss is approximately 5 dB. The best conversion loss measured was 4.8 dB. Figure 19 shows the conversion loss vs. local oscillator (LO) power for the 32.3-GHz mixer. Local oscillator

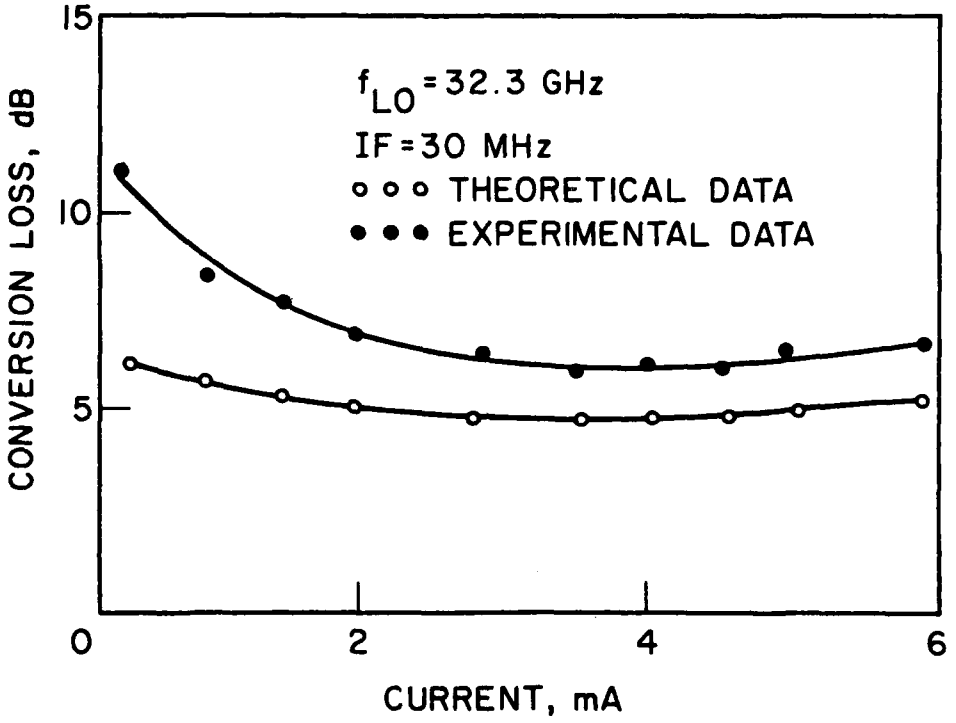

Figure 17. BARITT mixer conversion loss. (IF = 30 MHz)

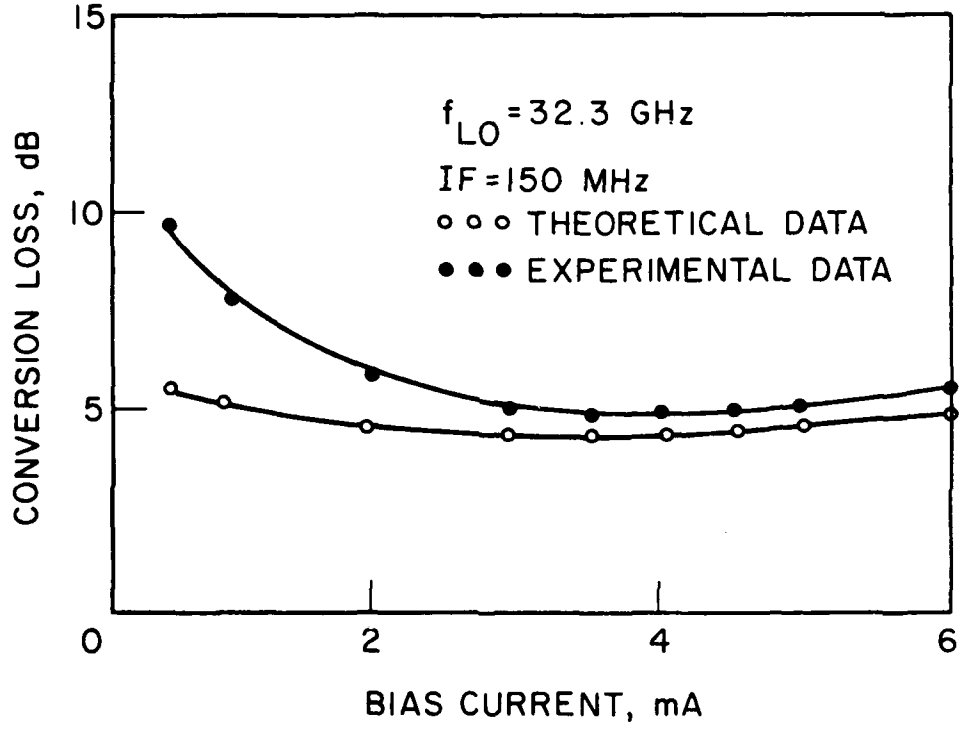

igure 18. BARITT mixer conversion loss. (IF = 150 MHz)

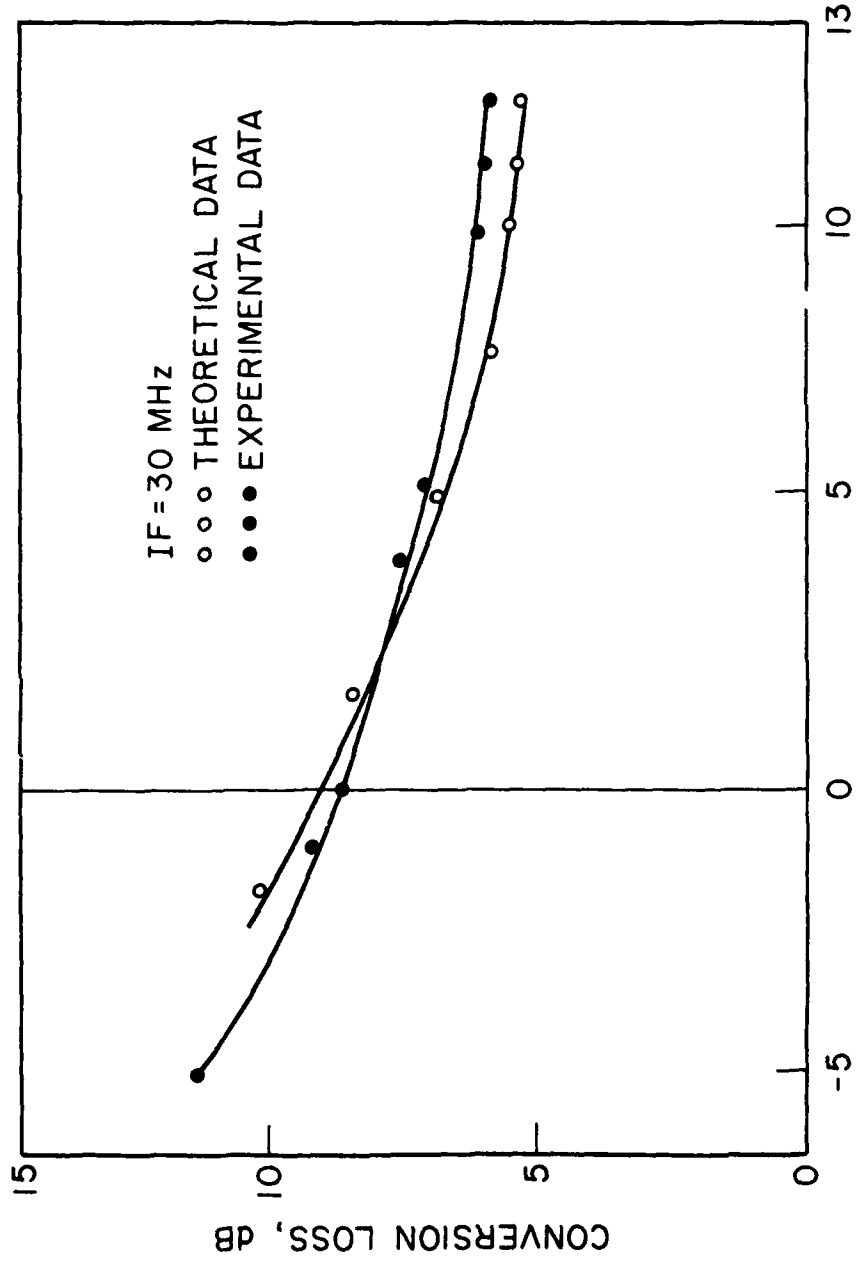

Figure 19. BARITT mixer conversion loss vs. local oscillator power.

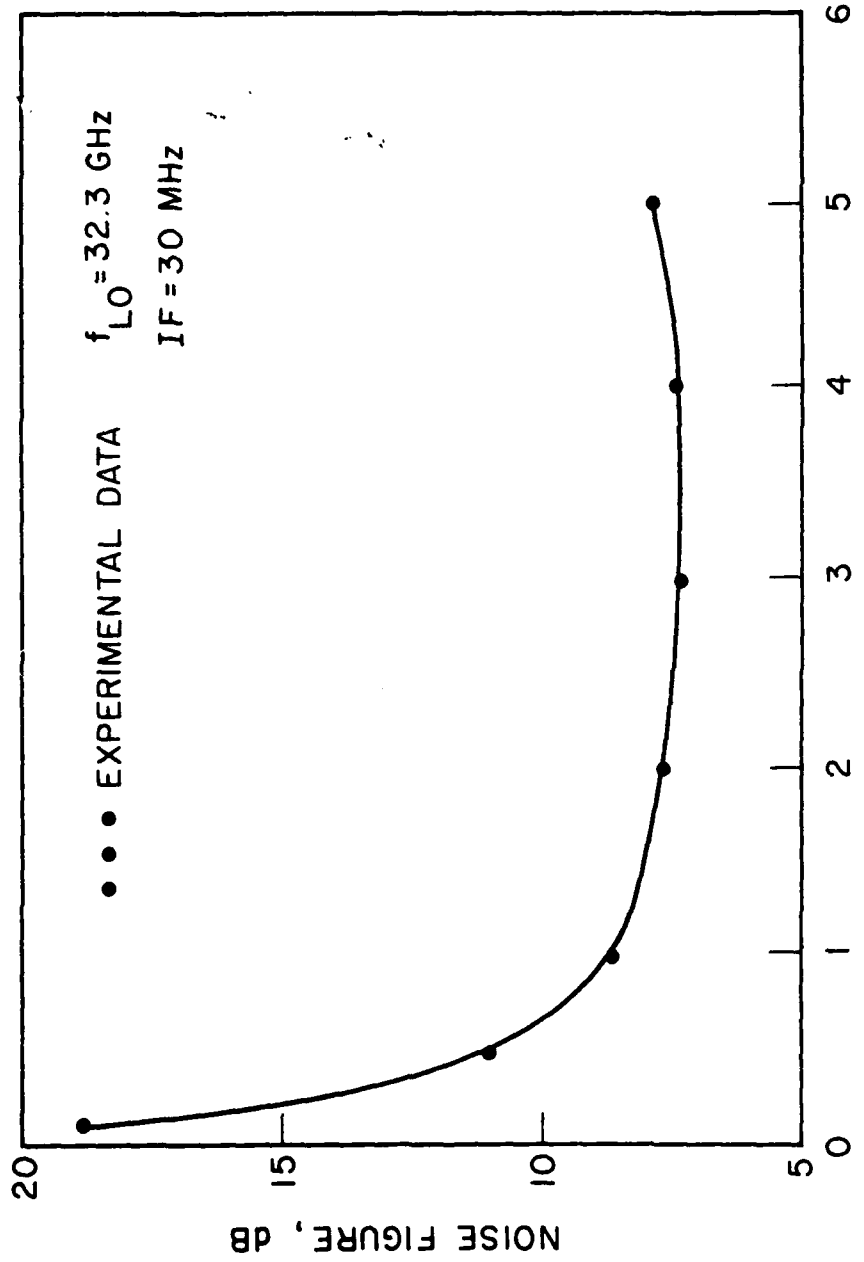

Figure 20. BARITT mixer noise figure.

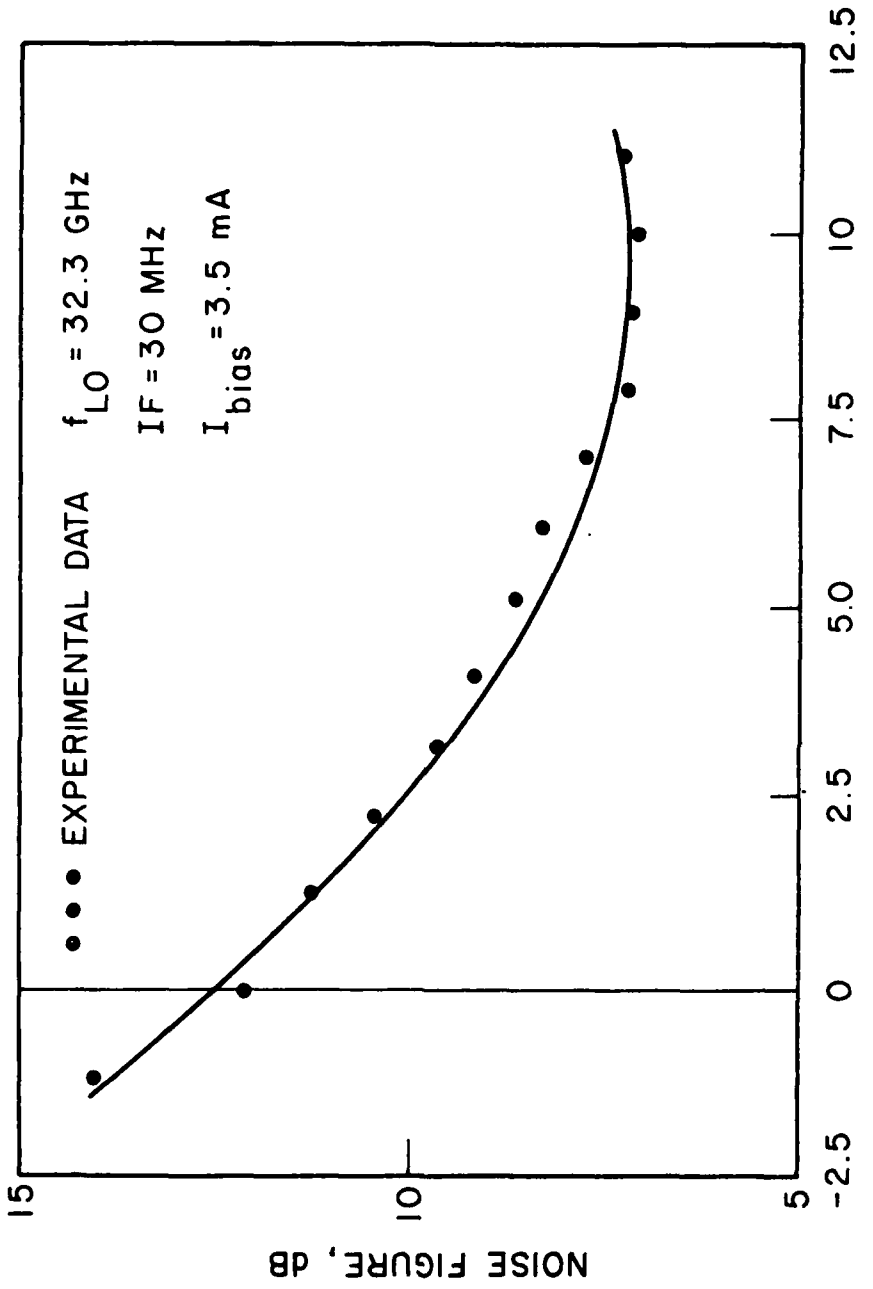

Figure 21. BARITT mixer noise figure.

pumps of 10 to 13 dBm result in the best conversion loss. Increasing the local oscillator power above 13 dBm increased the conversion loss. Figure 20 shows the BARITT mixer noise figure for the same 32.3-GHz signal, 30 MHz IF conditions were used to make conversion-loss measurements. The IF amplifier had a 2.5-dB noise figure. The noise figure measured was the same with the signal above or below the pump frequency so the noise figure shown in Figure 20 is the double-sideband noise figure. The noise figure with a 150-MHz IF was the same as with a 30-MHz IF. The noise figure vs. local oscillator power is shown in Figure 21. Local oscillator powers of 7 to 10 dBm produced the best mixer noise figure.

The data in Figures 17 through 21 show the basic performance to be expected from BARITT mixers. The conversion loss and noise figure of BARITT mixers are both several dB worse than for Schottky mixers. With further work on the device and the circuit both numbers could be improved. However, because of the BARITT structure, the noise performance will always be slightly worse than the best Schottky mixers.

Preliminary measurements were also obtained on 95-GHz detector structures. These diodes were fabricated fron $n\text{-}p^+$ wafers with a specified n-layer doping of 2.5×10^{16} cm^{-3} and n-layer thickness of 1.4 μm. A p^+ contact diffusion reduced the layer thickness to approximately 0.6 μm. The diodes had the multijunction structure and were tested in the point contact cavity shown in Figure 9. These diodes had the same graded substrate epitaxial layer interface as the 35-GHz devices. The V-band detector results are shown in Figures 22 and 23. These diodes had a contact diameter of 12.5 μm and an operating voltage of 7 V. The video amplifier bandwidth was

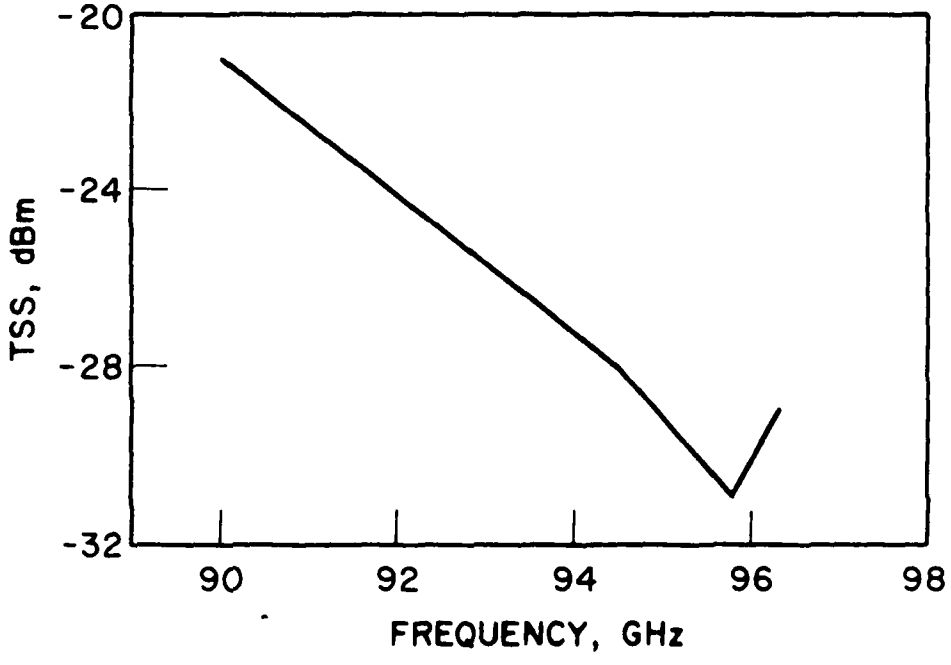

Figure 22. BARITT detector TSS vs. frequency.

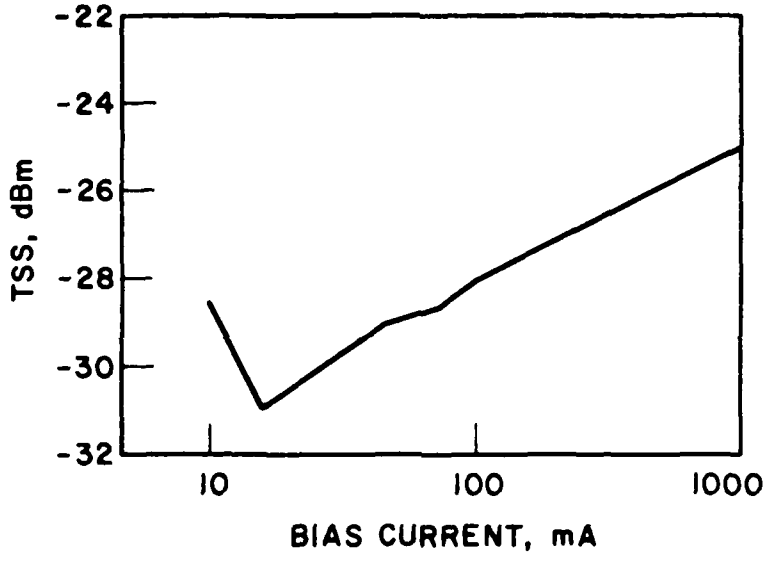

Figure 23. BARITT detector TSS vs. bias current.

1 MHz. The best V-band TSS was - 31 dBm at 95.8 GHz with a bias current of 20 μA. Additional work would be needed to find the limits of BARITT devices at V-band frequencies.

6. GaAs TUNNETT FABRICATION AND RESULTS

A second area of work on this program was the fabrication and evaluation of GaAs TUNNETT devices for use as millimeter-wave mixers and detectors. There were difficulties getting the proper material for these devices. However, several TUNNETT structures were fabricated and tested. TUNNETT fabrication and experimental results were discussed in this section.

The fabrication steps for 94-GHz TUNNETT diodes are shown in Figure 24. The starting material is n-n^+ GaAs with an epitaxial layer thickness of 0.45 μm and a doping of 5×10^{16} cm^{-3}. The desired structure is a metal-n^+-n-n^+ structure with the n^+ front layer chosen to give a tunneling breakdown. However the amount of dopant in the n^+-layer required is difficult to calculate or control, so an experimental approach was taken. The wafer was ion implanted with a dose of 2×10^{13} cm^{-2} at 200 keV. After annealing, a heavily doped activated layer is present at the surface. The cap is then removed and the I-V characteristic of the diode is measured. The initial breakdown voltage is low because the junction depletion layer does not extend to the n-layer before the field at the interface becomes high enough to allow tunneling. Some of the surface can be removed by anodic etching. This lowers the thickness of the n^+-layer and increases the breakdown voltage. By removing

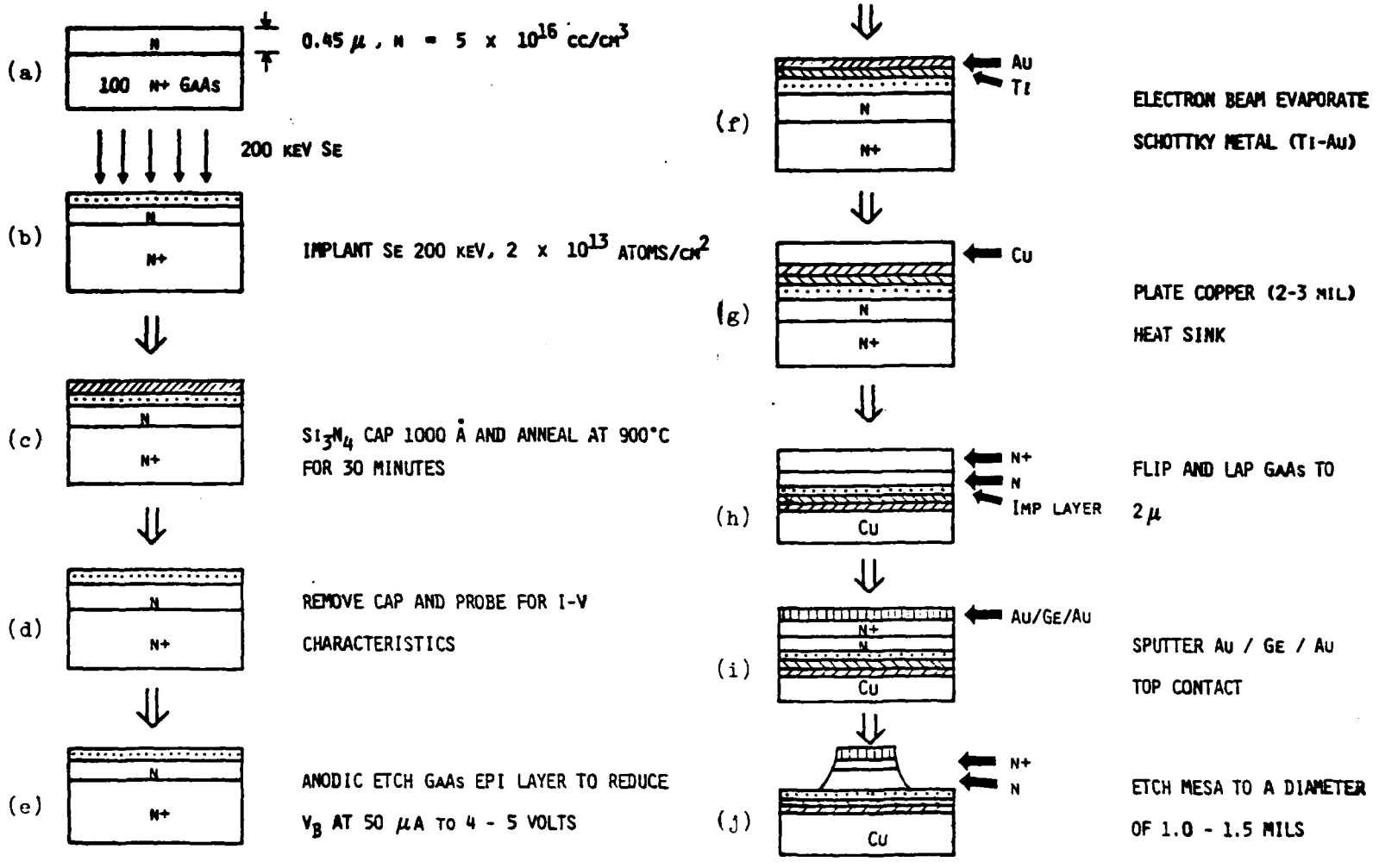

Figure 24. Fabrication steps for 94-GHz TUNNETT diodes.

thin layers and remeasuring the breakdown voltage, the required n^+-layer thickness will be obtained. The required thickness occurs when the junction depletion layer extends through the n-layer to the $n\text{-}n^+$ substrate interface. When this happens the breakdown voltage will increase from relatively small values to approximately 5 V. The wafer is then ready for further processing. The wafer is first metallized with Ti and gold to form Schottky barriers. Copper heat sinks are then plated. The entire structure is then turned over and the substrate is lapped away giving a 2-μm thick structure. The back contact is formed with Au/Ge and the wafer is mesa etched to produce the finished structure. The I-V characteristic of a completed device is shown in Figure 25. The device I-V characteristics were measured as a function of temperature to determine the type of current injection. The forward and reverse characteristics at room temperature and at 77° are shown in Figure 26. The breakdown voltage increases with decreasing temperature indicating a tunneling injection.

The TUNNETT devices were tested as detectors at 94 GHz in a reduced-height waveguide circuit. The TUNNETT detector had a TSS of - 34 dBm (per 300 kHz at a bias current of 10 μA).

There were several problems with the fabrication and evaluation of the TUNNETT devices. The TUNNETT is more difficult to fabricate than the BARITT device. Also, the 94-GHz circuit was more difficult to use. The diode had to be bonded onto a microstrip line and contacted with a small wire. The BARITT devices were tested in a different circuit which was designed after seeing the problems of the TUNNETT.

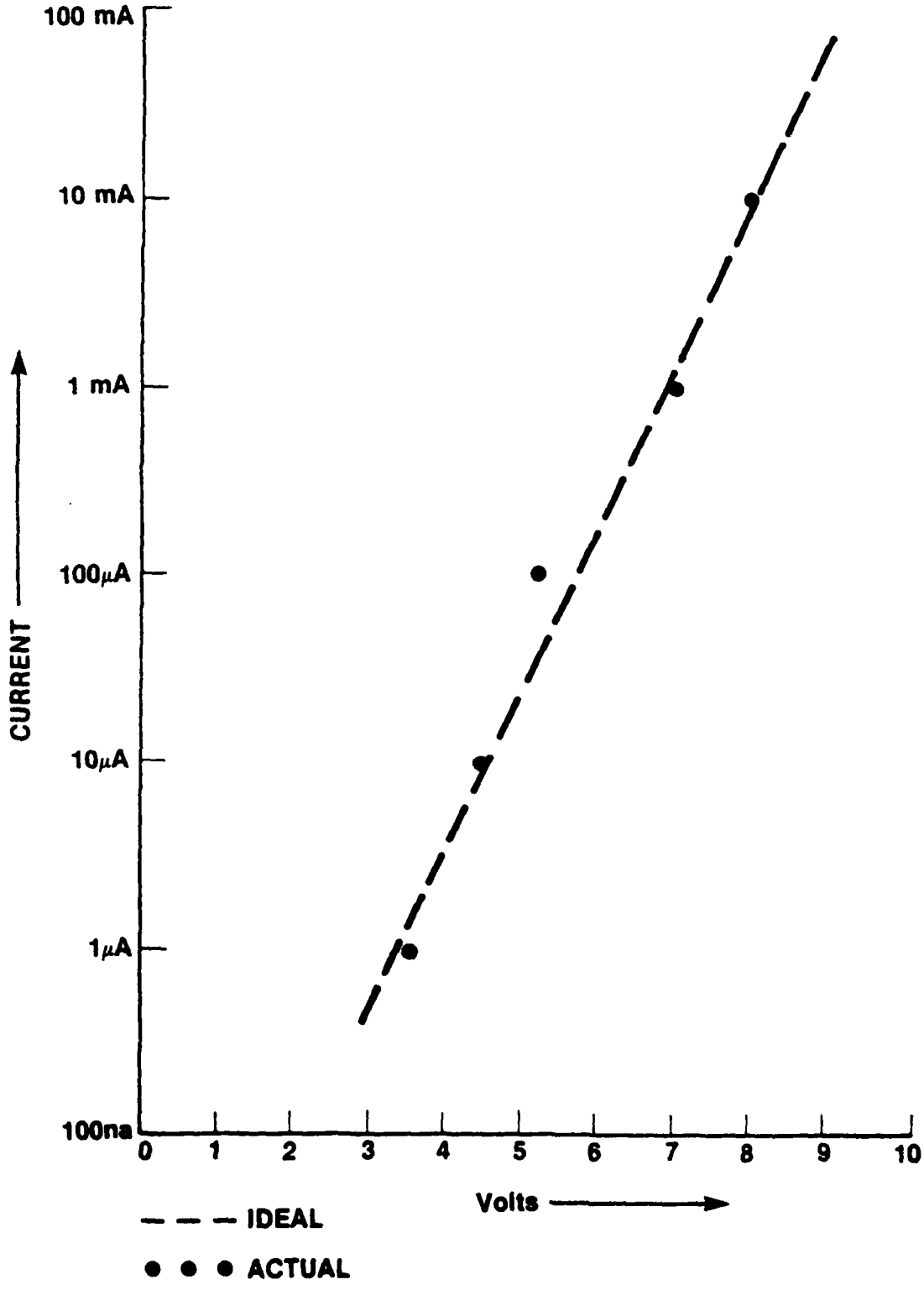

Figure 25. Dc characteristics of TUNNETT devices.

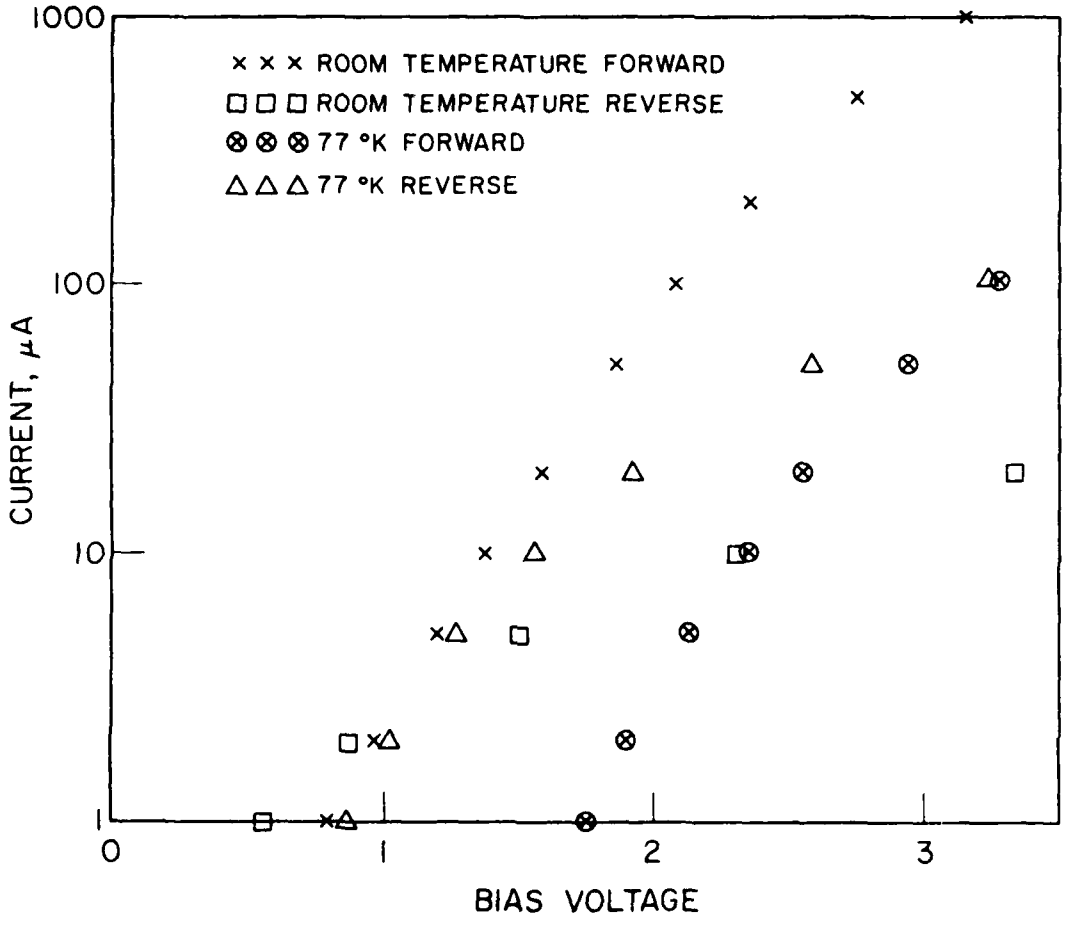

Figure 26. I-V characteristics of TUNNETT devices.

7. SUMMARY AND CONCLUSIONS

Several fabrication methods were developed for Si BARITT devices operating at 35 and 95 GHz. A large number of these devices have been RF tested as mixers and detectors. The BARITT has proven to be a useful detector at 35 GHz with TSS performance comparable to Schottky detectors, while the burnout performance and the dynamic range are superior. BARITTs have reasonable mixer performance. The conversion loss is good and the noise figure is within 3 dB of a Schottky mixer. These numbers, combined with the excellent pulse burnout performance, make the BARITT device useful in radar systems and receiver front ends. When limiter losses in Schottky mixer systems are included, the BARITT and Schottky devices have comparable performance. BARITT performance at 95 GHz was also encouraging. Preliminary detector TSS measurements gave a TSS of - 31 dBm per 1 MHz bandwidth. These performance figures combined with the ease of fabrication and potential for low cost make the BARITT an important millimeter-wave device.

END

DATE
FILMED

1-84

DTIC